Article

Improving GNSS-IR Sea Surface Height Accuracy Based on a New Ionospheric Stratified Elevation Angle Correction Model

Jiadi Zhu [1,†]**, Wei Zheng** [1,2,3,*,†]**, Yifan Shen** [3,†]**, Keke Xu** [1] **and Hebing Zhang** [1]

1   School of Surveying and Land Information Engineering, Henan Polytechnic University, Jiaozuo 454003, China;
    212204010017@home.hpu.edu.cn (J.Z.); xkk@hpu.edu.cn (K.X.); jzitzhb@hpu.edu.cn (H.Z.)
2   School of Electronics and Information Engineering, Harbin Institute of Technology, Weihai 264209, China
3   School of Geomatics, Liaoning Technical University, Fuxin 123000, China; shenyifan@lntu.edu.cn
*   Correspondence: wzheng@xidian.edu.cn
†   These authors contributed equally to this work.

Abstract: Approximately 71% of the Earth's surface is covered by vast oceans. With the exacerbation of global climate change, high-precision monitoring of sea surface height variations is of vital importance for constructing global ocean gravity fields and preventing natural disasters in the marine system. Global Navigation Satellite System Interferometry Reflectometry (GNSS-IR) sea surface altimetry is a method of inferring sea surface height based on the signal-to-noise ratio of satellite signals. It enables the retrieval of sea surface height variations with high precision. However, navigation satellite signals are influenced by the ionosphere during propagation, leading to deviations in the measured values of satellite elevation angles from their true values, which significantly affects the accuracy of GNSS-IR sea surface altimetry. Based on this, the contents of this paper are as follows: Firstly, a new ionospheric stratified elevation angle correction model (ISEACM) was developed by integrating the International Reference Ionosphere Model (IRI) and ray tracing methods. This model aims to improve the accuracy of GNSS-IR sea surface altimetry by correcting the ionospheric refraction effects on satellite elevation angles. Secondly, four GNSS stations (TAR0, PTLD, GOM1, and TPW2) were selected globally, and the corrected sea surface height values obtained using ISEACM were compared with observed values from tide gauge stations. The calculated average Root Mean Square Error (RMSE) and Pearson Correlation Coefficient (PCC) were 0.20 m and 0.83, respectively, indicating the effectiveness of ISEACM in sea surface height retrieval. Thirdly, a comparative analysis was conducted between sea surface height retrieval before and after correction using ISEACM. The optimal RMSE and PCC values with tide gauge station observations were 0.15 m and 0.90, respectively, representing a 20.00% improvement in RMSE and a 4.00% improvement in correlation coefficient compared to traditional GNSS-IR retrieval heights. These experimental results demonstrate that correction with ISEACM can effectively enhance the precision of GNSS-IR sea surface altimetry, which is crucial for accurate sea surface height measurements.

Keywords: new ionospheric stratified elevation angle correction model; sea surface altimetry; GNSS-IR; SNR; ionospheric refraction correction

1. Introduction

The oceanic gravity field serves as a crucial foundational dataset for areas such as seafloor topography inversion, marine resource exploitation, and elevation datum standardization [1]. Satellite altimetry technology can "directly" measure the oceanic geoid surface and utilize the functional relationship between the geoid surface and gravity anomalies to invert oceanic gravity anomalies [2]. Therefore, satellite altimetry technology has become one of the primary means for inverting the oceanic gravity field [3]. Over the past few decades, sea surface altimetry has evolved from traditional manual data collection on ships and tidal gauge measurements to satellite altimetry and now to the developing stage of Global Navigation

Satellite System reflectometry (GNSS-R). The advancement of these technologies has not only enhanced the accuracy and coverage of sea surface altimetry but also provided rich data support for ocean science, climate research, marine management, and other fields [4]. In summary, sea surface height inversion provides both quantitative and qualitative descriptions of changes in ocean surface height. It is a crucial ocean observation technology that holds significant importance for various marine activities and research endeavors.

In the 1960s, the United States first proposed pioneering research on the Global Navigation Satellite System (GNSS). Subsequently, systems such as the Soviet Union's GLONASS, Europe's GALILEO, and China's BeiDou were successively developed [5,6]. As of now, there are over 100 operational navigation satellites globally, offering advantages such as high precision, all-weather capability, and rich signal diversity. In 1993, Martin-Neria first proposed using GNSS reflection signals for medium-scale sea surface height measurements, thereby providing robust data support for global gravity field observations, known as GNSS-R for sea surface altimetry [7]. Following this, researchers conducted airborne experiments and collected data using spaceborne imaging radar in the C-band, both of which detected reflection signals [8,9]. Subsequently, comprehensive research began on utilizing GPS reflection signals for elevation measurements [10]. Between 1997 and 2006, Martin-Neira and colleagues conducted the PARIS (Passive Reflectometry and Interferometry System) altimeter experiments at the Zeeland Bridge in the Netherlands. These experiments, divided into PARIS Bridge I, Bridge II, and Bridge III, involved using shore-based receivers. In all three experiments, sea surface heights were successfully retrieved. Among them, the results of the Bridge III experiment were particularly noteworthy, with measurement errors of less than 10 cm [11–13]. The development of shore-based systems significantly increased the efficiency of sea surface height measurements. This led to the advancement of airborne GNSS-R altimetry and spaceborne GNSS reflection measurements, greatly expanding the scope of sea surface altimetry and enhancing its accuracy [14,15]. With the continuous improvement of GNSS-R theoretical frameworks, signal processing techniques, and parameter inversion models, significant progress has been made in various fields. These include sea surface wind field monitoring [16–18], ocean altimetry [19], sea ice detection [20], snow depth measurement [21–23], sea ice remote sensing [24–26], the monitoring of oil spills on the ocean surface [27–29], surface water measurement [30,31], and soil moisture measurement [32,33].

Even though GNSS-R has advantages such as all-weather, all-time, and multi-signal sources [34,35], the proposed time is also relatively early [7]. However, its slow development, difficulty in data acquisition, requirement for dual-antenna receivers, susceptibility to signal polarization effects, and other drawbacks increase costs. Consequently, the use of GNSS-IR for sea surface height measurement has been proposed. GNSS-IR technology only requires traditional geodetic receivers to accomplish height monitoring. Based on the frequency characteristics within the signal-to-noise ratio (SNR), it can achieve reflection surface height change monitoring. This approach offers advantages such as full automation, low cost, long-term continuity, and a fixed framework [36,37]. In 2013, Larson et al. introduced the method of LSP analysis for sea surface height measurements, comparing computed results with nearby tide gauge stations. The root mean square error was less than 5 cm, and the correlation coefficient reached 0.97 [38]. In 2014, Loefgren et al. analyzed the signal-to-noise ratio observations from five GPS stations at the Onsala GTGU in Sweden. They obtained high-precision sea level height results, with a correlation of 0.89–0.99 to the sea level heights observed using traditional tide gauges at the same location [39]. During signal propagation, ionospheric and tropospheric influences inevitably cause the refraction of satellite signals, impacting the precision of GNSS-IR height measurements. Subsequently, the study focused on variations in SNR oscillation frequencies at low elevation angles primarily attributed to the geometric bending of radio waves through the troposphere. Addressing these effects led to achieving a sea surface height accuracy of 10 cm [40]. In 2017, Larson et al. computed the impact of tropospheric refraction on the elevation angles

of GNSS-IR sea level height measurements. They found that the root mean square error between tide gauge measurements and GNSS-IR data was 12 cm [41].

The atmospheric refraction effect will cause signal bending, which will lead to the deviation between the calculated elevation angle and the actual elevation angle, and this elevation angle deviation will further lead to the deviation of GNSS-IR sea surface altitude inversion results. The atmospheric refraction effect encompasses both tropospheric and ionospheric refraction. Regarding the troposphere, Santamria et al. employed a refraction correction formula to mitigate the elevation angle bias induced by atmospheric refraction, significantly enhancing the accuracy of inversion measurements [40]. Williams et al. utilized the VMF1 mapping function model and GPT2w tropospheric delay model to correct tropospheric delay errors, thereby achieving more accurate tidal amplitude estimates [42]. The research of troposphere in GNSS-IR sea surface altimetry has resulted in a higher correction of sea surface altimetry. In the ionosphere, the existence of these ionized charged particles will inevitably affect the passing electromagnetic wave, causing it to refract, group delay, and other phenomena. The refraction of the satellite signal causes the apparent distance and elevation angle of the target measured by the satellite to deviate from the real distance and elevation angle [43], resulting in the height inversion value of the GNSS-IR sea surface deviating from the real value. However, studies on the ionosphere in GNSS-IR sea surface height measurement are scarce. Therefore, it is necessary to correct the ionospheric refraction error of satellite signals in order to accurately measure the sea surface height of GNSS-IR.

Different from previous studies, this article focuses on the ionospheric refraction of satellite signals along the propagation path and constructs a new model for correcting the elevation angles of the satellite signals. First, GNSS observation data files obtained from receivers are used to calculate the satellite's elevation angle, azimuth angle, and signal-to-noise ratio (SNR). Due to the uneven distribution of electron density in the ionosphere, the ionosphere is stratified according to the International Reference Ionosphere (IRI) model. Based on the electron density of each layer, elevation angle correction values are calculated using the ray tracing method. Finally, accurate sea surface heights are obtained after correction through the ionospheric stratified elevation angle correction model. The corrected results are compared with tide gauge station measurements to evaluate the method's reliability using root mean square error (RMSE) and Pearson correlation coefficient (PCC).

2. Construction of the New Ionospheric Stratified Elevation Angle Correction Model

2.1. Ionosphere Layering Design

The ionosphere of the Earth is a region of the upper atmosphere about 60 km to 1000 km above the Earth, which is partially ionized due to the influence of polar ultraviolet rays and X-rays. According to the degree of ionization and electron density, the ionosphere can usually be divided into four layers, respectively, the D layer (60~90 km, usually disappear at night), E layer (90~140 km), F1 layer (140~210 km, often disappear at night), and F2 layer (more than 210 km, the lowest atmospheric density of the layer. The particle collision binding rate is the lowest, and the maximum electron density usually occurs in this layer. At the same time, this layer is also the main area that affects the transmission of satellite signals) [44].

Research on electron density in the ionosphere has become relatively mature, with various computational models available. For example, the Global Positioning System (GPS) initially used the Klobuchar model to correct ionospheric delay, and the European Union's Galileo navigation system employs the three-dimensional electron density model (NeQuick G) for ionospheric delay correction. The International Reference Ionosphere (IRI) is a project initiated by the Committee for Space Research (COSPAR) and the International Union of Radio Science (URSI). Its objective is to develop empirical standard models of the ionosphere based on various available data sources. This model can provide the electron density of the ionosphere without aurora for specific times and locations under

geomagnetically quiet conditions. Currently, the IRI is recognized as the international standard for electron density and temperature specifications [45]. By inputting parameters such as time, latitude, longitude, and altitude, users can obtain a wealth of ionospheric parameters crucial for physics, including electron density from 60 to 2000 km altitude, the peak electron density of the F2 layer (NmF2), the peak height of the F2 layer (HmF2), ion temperature, and Total Electron Content (TEC). Therefore, this study utilized the IRI model to extract ionospheric electron density content.

As this study subsequently selected GNSS stations in Spain, Australia, and the United States, electron density maps were generated for these regions across various times and seasons. This was undertaken to explore the selection of upper and lower bounds for ionospheric layer heights. According to the literature [46], the electron density in the ionosphere exhibits significant variations over time due to diurnal cycle and seasonal effects. Incorporating numerous layers can extend the extraction time for electron density data. Figure 1 shows that the distribution of electron content density in the ionosphere is mainly concentrated in the vicinity of 100~450 km. Considering that the refraction of satellite signals by the ionosphere is primarily determined by the electron density, regions of the ionosphere with lower electron density have less impact on the refraction of satellite signals [47]. In order to calculate the time and efficiency, this study applied the international reference ionospheric model (IRI), selected an ionospheric height of 100~450 km, and divided the ionosphere into eight layers with a step length of 50 km. The ionospheric refraction of satellite signals was studied, and the final influence of the ionosphere on the accuracy of GNSS-IR sea surface height inversion was explored.
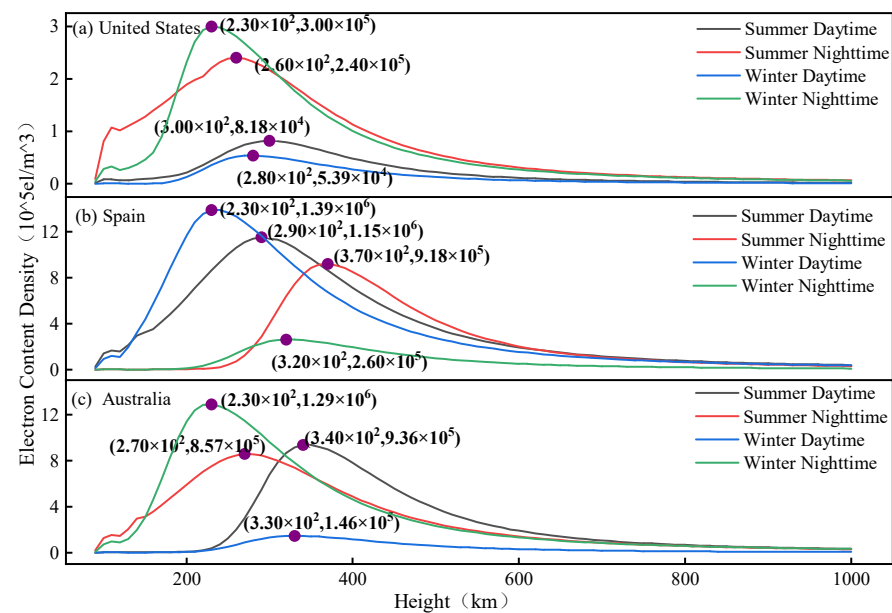

Figure 1. (**a**) The electron density map of the United States region; (**b**) the electron density map of the Spain region; (**c**) the electron density surface distribution map of the Australia region.

2.2. *The Train of Thought for the New Ionospheric Stratified Elevation Angle Correction Model*

The ray tracing method is employed to calculate the distance and angle of refraction experienced by satellite signals during propagation. Derived rigorously from Snell's law and Fermat's principle based on mathematical geometric relationships, this method exhibits high precision and has consequently become a widely adopted correction technique in engineering applications [48]. In GNSS-IR shore-based sea surface surveys, there remains a lack of robust solutions for mitigating the effects of ionospheric refraction on satellite signal propagation. Moreover, the electron density within the ionospheric region exhibits non-uniform distribution across vertical height layers due to diurnal cycle, seasonal, and other environmental influences. The traditional ray tracing methods offer limited enhancement in

sea surface height retrieval accuracy through satellite elevation angle refraction calculations under a single-layer ionosphere. Therefore, this study extends the concept of traditional ray tracing by introducing a stratified ionospheric model, aimed at constructing a new ionospheric stratified elevation angle correction model for improved precision in sea surface height inversion.

The construction rationale of ISEACM is outlined as follows: Firstly, the azimuth angle and altitude angle of the satellite are calculated by using a GNSS observation data file and satellite orbit file, and the interference signal-to-noise ratio data of direct signal and reflected signal are extracted from the observation data file. Simultaneously, the satellite's PRN serial number and corresponding time are recorded, and these parameters are combined on a daily basis to generate signal-to-noise ratio data files. Secondly, taking into account the non-uniform distribution of electron density in the ionosphere and based on the analysis in Section 2.1, the ionospheric height range of 100 to 450 km was chosen. The ionosphere was divided into eight layers with a step size of 50 km. Using the satellite's elevation angle, azimuth, and the altitude of each ionospheric layer, the penetration point (longitude and latitude) of the ionosphere is calculated. Subsequently, the electron density of each layer is obtained using the IRI model. Thirdly, utilizing electron density values obtained from the IRI model, the elevation angle correction for each ionospheric layer is computed using the ray tracing method. To mitigate the influence of tropospheric refraction on satellite signal bending, a tropospheric refraction model was introduced to correct the refraction angles of satellite signals. The heights of the sea surface around the measurement stations were obtained using the LSP spectrum analysis method, and the results of height inversion underwent quality control. Consequently, the inversion results of GNSS-IR sea surface heights were obtained. Fourthly, tidal data from nearby tide gauge stations were obtained, and outliers in GNSS-IR sea surface height inversion were removed. Comparative analysis between tidal data and inversion height data was conducted. Ultimately, the accuracy of inversion data corrected by ISEACM was compared with uncorrected inversion data to evaluate the superiority of the proposed model in this study. The main research process is shown in Figure 2.
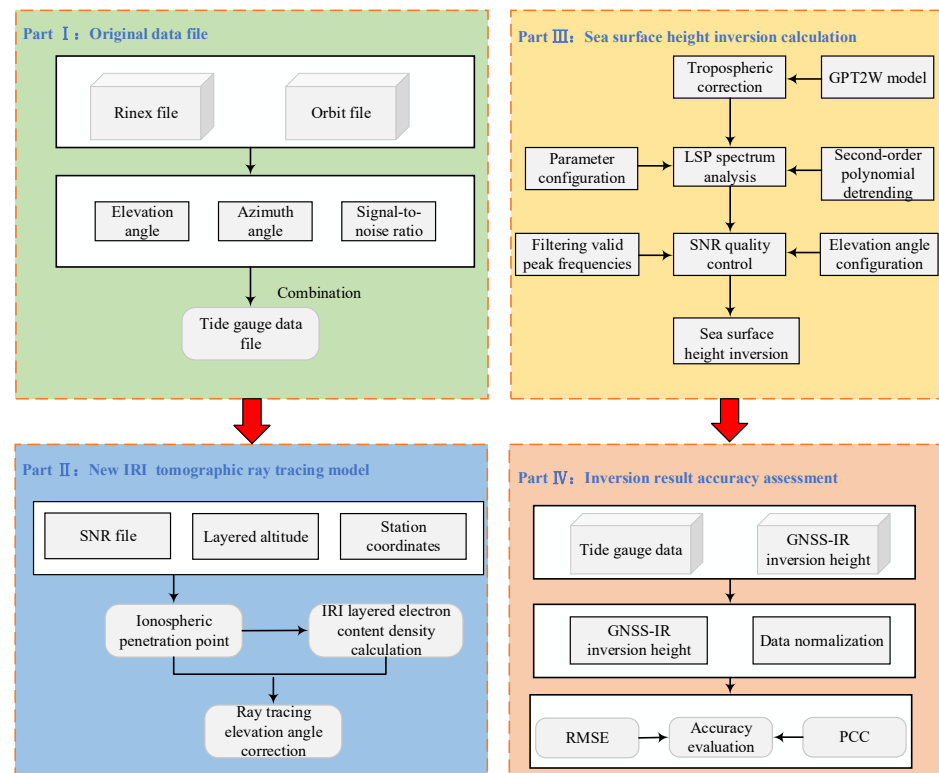
Figure 2. The flowchart of the new ionospheric stratified elevation angle correction model.

2.3. Construction of the New Ionospheric Stratified Elevation Angle Correction Model

In GNSS-IR sea surface height inversion measurements, the signals received by the satellite receiver primarily consist of direct signals from the satellite and reflected signals that have bounced off the sea surface before reaching the receiver. Ultimately, the vector sum of the direct and reflected signals is obtained [49]. The strength of the composite signal is expressed using the SNR, which is primarily influenced by factors such as multipath effects, signal transmission power, and antenna gain [50]. Figure 3 shows the basic schematic diagram of GNSS-IR sea surface height inversion, where H is the vertical distance from the phase center of the satellite receiver antenna to the sea surface; θ is the angle between the direct signal and the sea level—that is, the elevation angle of the satellite; and D is the additional distance of the reflected signal relative to the direct signal.
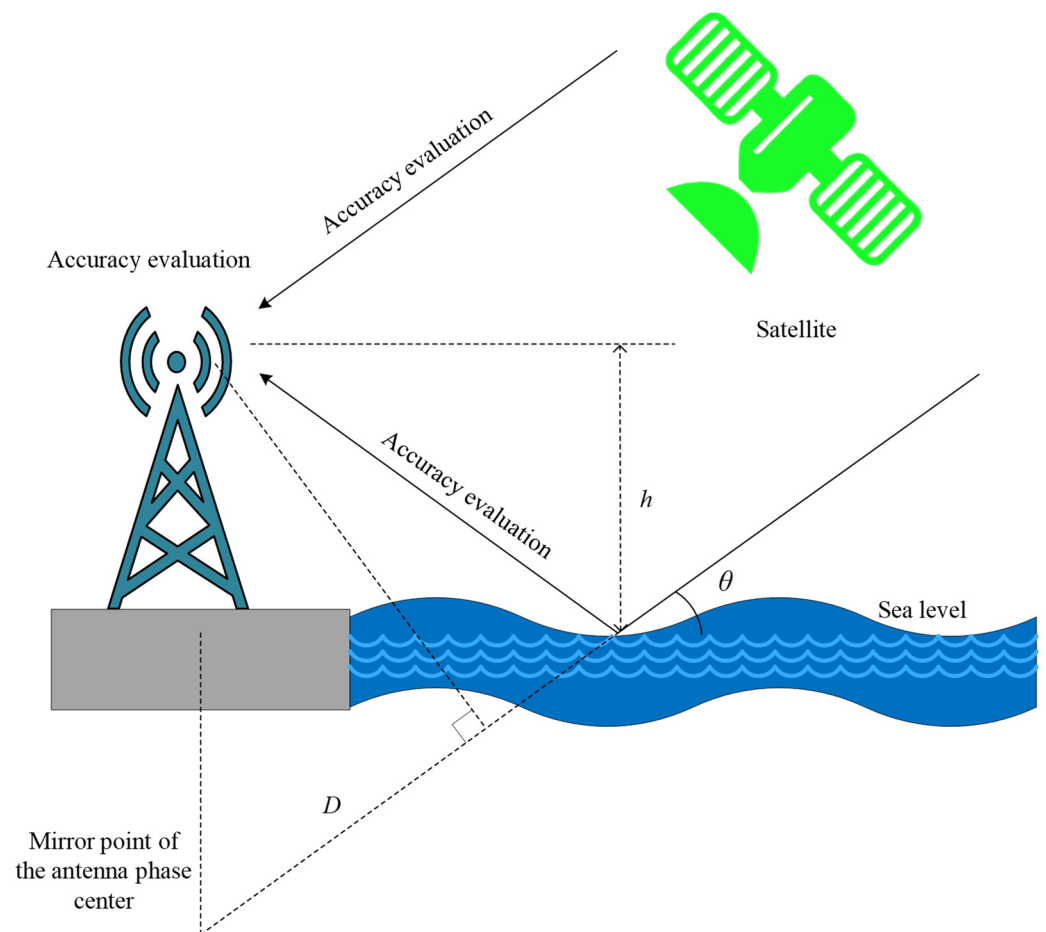
Figure 3. Basic principle diagram of GNSS-IR sea surface height measurement.

GNSS-IR refers to the reception of both direct and reflected signals from satellites by the receiver. These signals interfere with each other, as illustrated in Figure 3. The interference signal formed by the direct and reflected signals is recorded by the receiver within the signal-to-noise ratio (SNR), which can be described as follows [51]:

$$SNR^2 = A_d^2 + A_m^2 + 2A_d^2 A_m^2 \cos \varphi \tag{1}$$

where A_d^2 and A_m^2 are the amplitudes of the direct and reflected signals, respectively, and φ is the phase difference between the direct and reflected signals. To ensure accurate positioning, the antennas of standard geodetic measurement receivers are typically designed with specific characteristics to mitigate the multipath effects, thereby ensuring that the received signals satisfy the $A_d^2 \gg A_m^2$ relationship. Consequently, under the influence of the direct signal, the SNR sequence generally exhibits a parabolic trend.

At low elevation angles, the SNR values are smaller, and they are more affected by multipath effects, resulting in more significant periodic oscillations. Therefore, it is easier to extract SNR oscillation characteristic parameters at low elevation angles compared to high elevation angles. Although SNR sequences at higher elevation angles contain more complete information about the reflective surface, the useful information often becomes submerged in complex noise, making it difficult to extract accurately. In traditional GNSS-IR models, a quadratic polynomial is often used to fit the trend of the SNR curve. Then, the fitted term is subtracted from the SNR curve to remove the direct signal and a small amount of reflected signal, i.e., the term $A_d^2 + A_m^2$ in Equation (2). The resulting SNR oscillation term can be approximated as [52]:

$$SNR_m = 2A_dA_m \cos \varphi = A \cos(2\pi f x + \phi) \tag{2}$$

where A is signal amplitude, f is oscillation frequency, and ϕ is the phase. The phase difference φ between the direct signal and the reflected signal can be calculated from the additional distance D [51]:

$$\varphi = \frac{2\pi}{\lambda}D = \frac{4\pi h}{\lambda}\sin(\theta) \tag{3}$$

where λ is the wavelength of the carrier. From Equation (3), it can be observed that there is a linear relationship between the phase difference and the sine value of the satellite elevation angle $\sin(\theta)$ [51]:

$$2\pi f = \frac{4\pi h}{\lambda} \tag{4}$$

After simplifying Equation (4), we can obtain the relationship between the height h of the reflecting surface and the frequency f [38]:

$$h = \frac{\lambda f}{2} \tag{5}$$

where λ is the wavelength, and f is the frequency.

This study utilizes the electron density provided by the International Reference Ionosphere (IRI) model. Based on the frequency of satellite signals in the L1 band, the ionospheric refractive index is calculated [47]:

$$n = 1 - \frac{40.36N_e}{f^2} \tag{6}$$

where N_e is the electron density, and f represents the frequency of the satellite signal.

The study primarily conducts a eight-layer stratification process focused on the layer with the highest electron density. Starting from the top layer at 450 km altitude and moving downwards along the satellite signal propagation path, the layers are stratified with a step size of 50 km. The ray tracing method is employed to update the elevation angles at each layer height [53]. Ultimately, the corrected satellite elevation angle after ionospheric refraction correction is obtained. Initially, the refractive indices of the ionospheric layers at heights corresponding to the $i - 1$ and $i - 2$ layers are computed based on the electron density at those ionospheric heights. Then, using the refractive indices, the zenith angle with respect to the Earth's center is determined. Finally, the corrected satellite elevation angle is calculated based on this information:

$$\varphi_i = \int_{r_{i-2}}^{r_{i-1}} \frac{n_{i-2}r_{i-2} \cos e_{i-2} dr}{r\sqrt{n_{i-1}^2 r^2 - n_{i-2}^2 r_{i-2}^2 \cos^2 e_{i-2}}} \tag{7}$$

$$z = \frac{\pi}{2} - ar\sin(r_0 \sin(\frac{\pi}{2} - e)/r_2) \tag{8}$$

$$\beta_i = ar\cos(n_i r_i \cos(z)/n_{i-1}r_{i-1}) \tag{9}$$

$$\alpha_{\mathrm{i}} = \frac{\pi}{2} - \varphi_{\mathrm{i}} - \beta_{\mathrm{i}} \tag{10}$$

where n_{i-1} is the refractive index of the upper ionospheric layer, n_{i-2} is the refractive index of the lower ionospheric layer, r_{i-1} is the height from the Earth's center to the target plane of the $i - 1$ layer, r_{i-2} is the height from the Earth's center to the target plane of the $i - 2$ layer, e_{i-2} is the satellite elevation angle corresponding to the $i - 2$ layer, and i is the corresponding layer number, with the highest layer being $i = 8$. Taking into account the curvature of the Earth, it is convenient to iteratively compute the satellite elevation angle along the direction of satellite signal propagation in layers. Therefore, the study calculates the initial elevation angle from the observer's location to the height of 450 km at the top layer of the ionosphere. r_0 is the radius of the Earth, r_2 is the sum of 450 km height and the Earth's radius, and e is the initial satellite elevation angle from the observer's location. Based on the refractive index of each ionospheric layer calculated according to Formula (3), the corresponding refraction angles for adjacent layers are computed using Snell's law.

Combining the refraction angle from the previous layer with the Earth-centered angles of the current layer and the previous layer, the updated elevation angle for this layer is determined using the theorem of interior angles in a triangle. By iteratively applying Equations (7)–(10) to compute the elevation angle for the next layer, the satellite elevation angle corrected for ionospheric refraction is obtained. This process ultimately yields the precise satellite elevation angle corrected for ionospheric effects.

3. Validation and Application of the New Ionospheric Stratified Elevation Angle Correction Model

3.1. Experimental Data

This study utilized observational data files provided by global GNSS networks, selecting observational data from four stations: TAR0, GOM1, PTLD, and TPW2. The data were sampled at 30 s intervals, with one month of continuous observational data chosen for each station. The TAR0 station (latitude and longitude: 36.00, −5.60) is located in Tarifa, Spain, and is equipped with a LEICA GR25 geodetic measurement receiver and a LEIAR20 LEIM antenna. The GOM1 station (latitude and longitude: 28.08, −17.10) is located in San Sebastian de La Gomera, Spain, and is equipped with a LEICA GR50 geodetic measurement receiver and a LEIAR20 LEIM antenna. The PTLD station (latitude and longitude: −38.34, 141.61) is located in Portland, Australia, and is equipped with a LEICA GR25 geodetic measurement receiver and a LEIAT504GG SCIS antenna. The TPW2 station (latitude and longitude: 46.20, −123.77) is located in Puerto Morelos, USA, and is equipped with a SEPT POLARX5 geodetic measurement receiver and a TRM59800.80 SCIS antenna. The selection of tide stations is based on the geographical location of the corresponding GNSS station, and the tide station nearest to the GNSS-IR sea level altimetry experimental station is selected. Figure 4 shows the positions and respective Fresnel zones of four stations.

To validate the reliability of ISEACM, adjacent tide gauge stations were selected for each GNSS site to provide supplementary verification of GNSS-IR sea surface height inversion. Utilizing GNSS single-antenna interferometric measurement mode for receiving satellite signal data, satellite elevation angles are set to be within 30 degrees whenever possible. Excessive elevation angles can adversely affect the interferometric results, leading to increased measurement errors in sea surface height inversion. With regard to satellite elevation angle settings, this study conducted experiments with 10-degree intervals for four stations. The research revealed that different stations in various regions may require different elevation angle configurations, which could be influenced by local factors such as nearby anchored vessels, obstructive tall structures in proximity, or distance from the station area. Based on satellite imagery from Google Maps, the stations were divided into four quadrants, 0–90°, 90°–180°, 180°–270°, and 270°–360°, for configuration. Detailed parameter settings for the TAR0, GOM1, PTLD, and TPW2 stations are provided in Table 1.
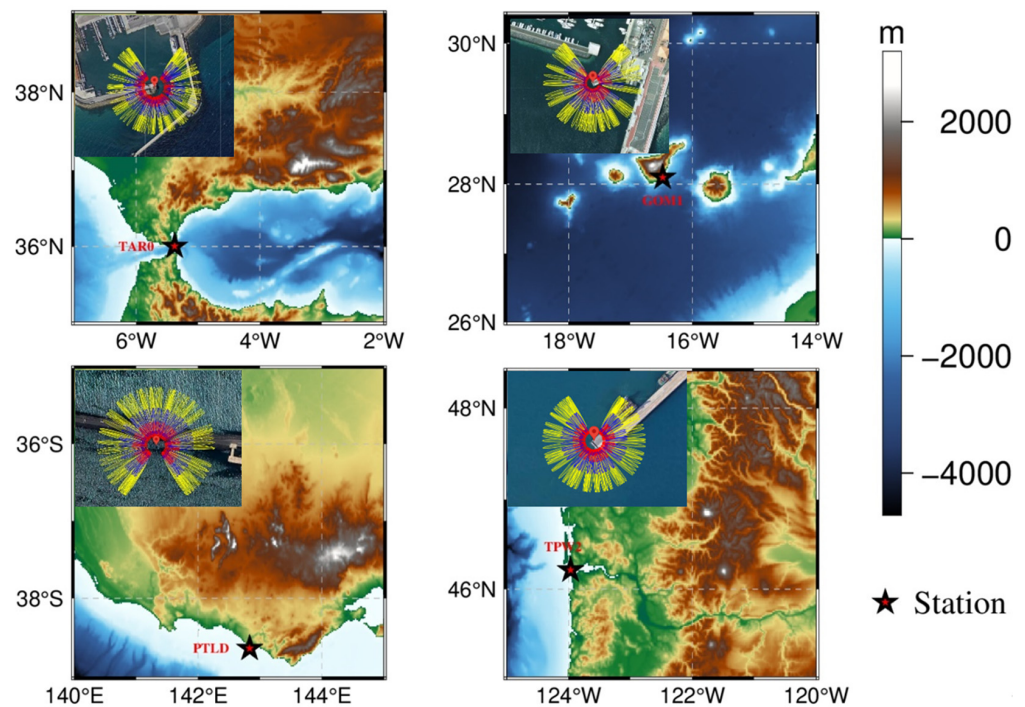
Figure 4. Distribution of GNSS stations and Fresnel reflection regions diagram.

Table 1. GNSS-IR station data information.

Station	Geographical Location	Sampling Interval (s)	Observation Duration (d)	Elevation Angle (°)	Azimuth Angle (°)	Tide Gauge Station	Distance (m)
TAR0	Spain	30	31	5–30	0–360	Tarifa	407.25
PTLD	Australia	30	31	5–30	0–360	Portland_AU	189.41
GOM1	Spain	30	31	5–30	0–360	LaGomera	6.52
TPW2	USA	30	31	5–30	0–360	ASTO	209.39

3.2. Accuracy Assessment Criteria

To demonstrate the superiority of the new ionospheric stratified elevation angle correction model, this study evaluates the accuracy of GNSS-IR sea surface height after correction by ISEACM compared to the original GNSS-IR sea surface height accuracy without model correction using the root mean square error (RMSE) and Pearson correlation coefficient (PCC).

The formula for the root mean square error (RMSE) is as follows [54]:

$$RMSE = \sqrt{\frac{1}{n}\sum_{i=1}^{n}(Y_i - X_i)^2} \tag{11}$$

where Y is the tidal gauge's sea level height measurement sequence, and X is the GNSS-IR sea surface height inversion results. The *RMSE* is used to assess the discrete deviation between the inversion results and the true values. A smaller root mean square error of the inversion height obtained after ISEACM correction indicates a more accurate inversion result after model correction.

The formula for Pearson's correlation coefficient, also known as Pearson's r, is as follows [55]:

$$PCC = \frac{\sum_{i=1}^{n}\left(X_i - \overline{X}\right)\left(Y_i - \overline{Y}\right)}{\sqrt{\sum_{i=1}^{n}\left(X_i - \overline{X}\right)^2}\sqrt{\sum_{i=1}^{n}\left(Y_i - \overline{Y}\right)^2}} \tag{12}$$

where $\overline{Y}$ and $\overline{X}$ are the means of the tidal gauge's sea level height measurement sequence and the GNSS-IR sea surface height inversion results sequence, respectively. *n* represents the number of data points in the sequences. *PCC* serves to depict the linear relationship between the sea level height sequence from tidal gauge measurements and the GNSS-IR sea surface height inversion results after model correction. Ranging from -1 to 1, *PCC* values closer to 1 signify more reliable inversion results.

3.3. Verification and Application of the New Ionospheric Stratified Elevation Angle Correction Model

This study utilized continuous GNSS observation data from four stations—TAR0, PTLD, GOM1, and TPW2—over a period of 30 consecutive days. The obtained results include continuous sea surface height inversion over 30 days, corrected using a new ionospheric stratified elevation angle correction model. Due to potential variations in reference levels among tidal gauge stations in different regions, the GNSS-IR-retrieved sea surface height inversions were normalized. Subsequently, comparative analysis was conducted with data from nearby GNSS stations and tidal gauge stations.

The entire process of GNSS-IR sea surface altimetry involves the transmission of satellite signals, their propagation through space, and their eventual reception by GNSS receivers. Each stage introduces varying degrees of measurement error. This study's ISEACM model primarily focuses on correcting the elevation angle variations in satellite signals caused by the ionosphere. A lower satellite elevation angle implies that the signal propagates a greater distance horizontally, so the ionosphere refracts the satellite signal more, which ultimately causes the measured elevation angle to deviate more from the true value. Employing low-elevation SNR data, this study focuses on investigating the precision impact of elevation angle correction on the final GNSS-IR sea surface height retrieval. To achieve this, daily data results from each experimental station were meticulously selected for detailed analysis and study.

Figure 5 is the deviation plots of elevation angles before and after correction using the novel ionospheric stratification elevation angle correction model. The horizontal axis represents the satellite elevation angle, while the vertical axis denotes the difference between elevation angles corrected by ISEACM and those without correction. The magnified line plot details the refraction corrections at each angle. As can be seen from Figure 5, the height angle correction of the four stations is basically between 0.05° and 0.21°.

Due to the long distance between the satellite and the receiver station, small changes will have a greater impact on the application of GNSS, so all error effects must be considered in the design. However, in GNSS-IR sea surface height retrieval experiments, the refraction effects of satellite signals in the ionosphere were not adequately taken into account. This resulted in deviations between computed satellite elevation angles and actual elevation angles, thereby reducing the accuracy of GNSS-IR sea surface height retrieval. Based on experimental results, it is evident that as the elevation angle increases, the angle corrected by ISEACM decreases. Conversely, at lower elevation angles, the correction to satellite elevation angles increases. This aligns with the relationship between elevation angle and propagation distance. These findings provide a solid basis for enhancing the accuracy of GNSS-IR sea surface height retrieval through ionospheric refraction corrections in future studies.

After applying error correction using the new ionospheric stratified elevation angle correction model, Figure 6 clearly shows a favorable correspondence between the inverted water levels from TAR0, PTLD, GOM1, and TPW2 stations and the measured water level results. This highlights the effectiveness of the ISEACM approach in correction. For the four stations mentioned above, the RMSE between the height retrieval results corrected by the new ionospheric stratified elevation angle correction model and the measurements from tide gauge stations are as follows: 0.1493 m for TAR0, 0.1732 m for PTLD, 0.2480 m for GOM1, and 0.2189 m for TPW2.
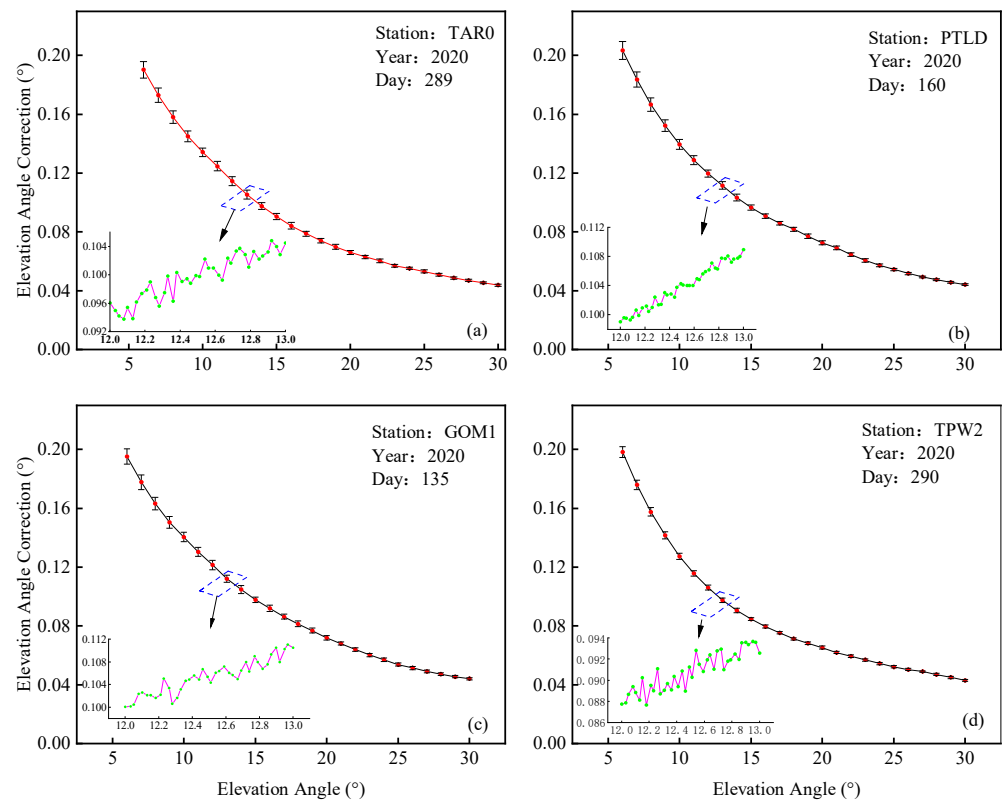
Figure 5. Diagram of angle correction quantities for ionospheric stratified elevation angle correction model stations: (**a**) The angular correction for TAR0 station; (**b**) The angular correction for PTLD station; (**c**) The angular correction for GOM1 station; (**d**) The angular correction for TPW2 station.
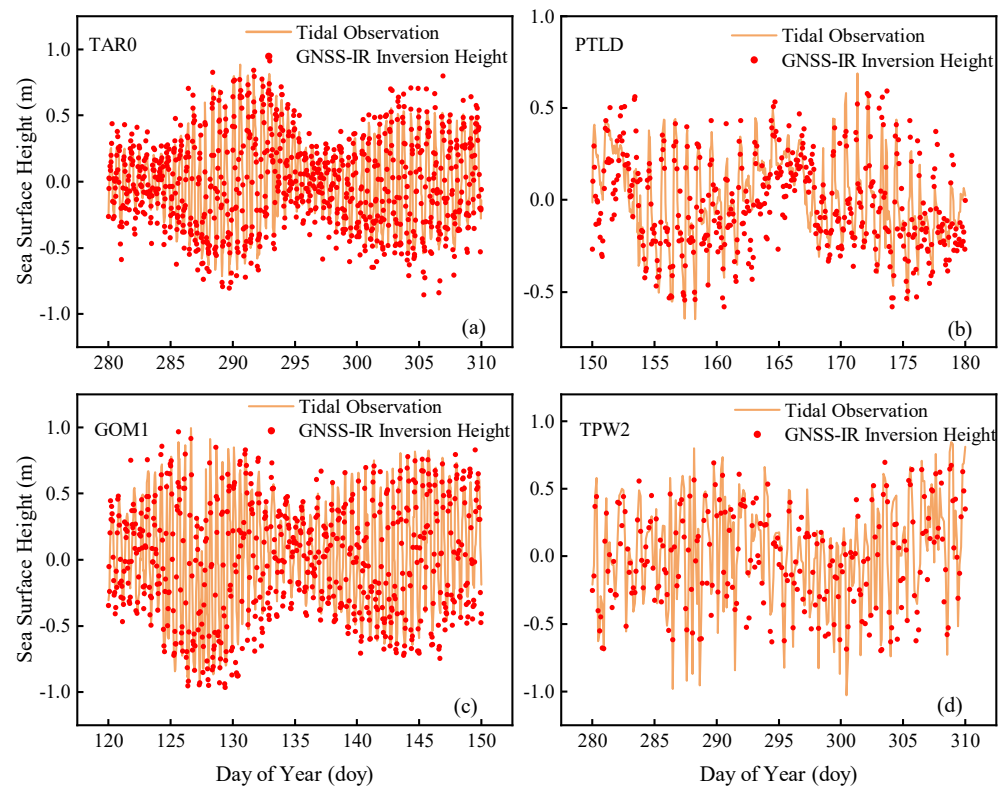
Figure 6. Comparison between the inverted height sequence values after correction using the ionospheric stratified elevation angle correction model and the observed tidal sequence values: (**a**) TAR0 station; (**b**) PTLD station; (**c**) GOM1 station; (**d**) TPW2 station.

Among these results, the TAR0 station exhibits superior inversion performance, showing the highest agreement with tidal observations. This can be attributed to its location on a solitary coastline with predominantly open sea surroundings, resulting in a high signal-to-noise ratio for satellite signals and a greater availability of data. Due to minimal influence from sea surface waves and relatively calm water conditions, the observed root mean square error is smaller. In contrast, the PTLD station is situated in a region of Australia that is farther from the coastline, surrounded by seawater, and subject to significant sea wind effects. Consequently, the data retrieved from GNSS-IR sea surface height inversion are more scattered, with fewer effective height data points available, resulting in a comparatively poorer overall height inversion performance compared to TAR0.

Through GNSS-IR sea surface height inversion experiments conducted at four stations, scatter plots of varying colors depict the correlation analysis of the novel ionospheric stratified elevation angle correction model. The horizontal axis is tidal observations from tide gauge stations, while the vertical axis is height values retrieved from GNSS-IR sea surface height inversion corrected by ISEACM. The Pearson correlation coefficients for each station are as follows: TAR0 station at 90.50%, PTLD station at 76.34%, GOM1 station at 84.70%, and TPW2 station at 83.84%. Figures 6 and 7 demonstrate that the sea surface height inversion values corrected using the ISEACM method exhibit a strong correlation with tidal observations from tide gauge stations. This indicates the reliability of ISEACM in ionospheric refraction correction research within GNSS-IR sea surface height measurements.
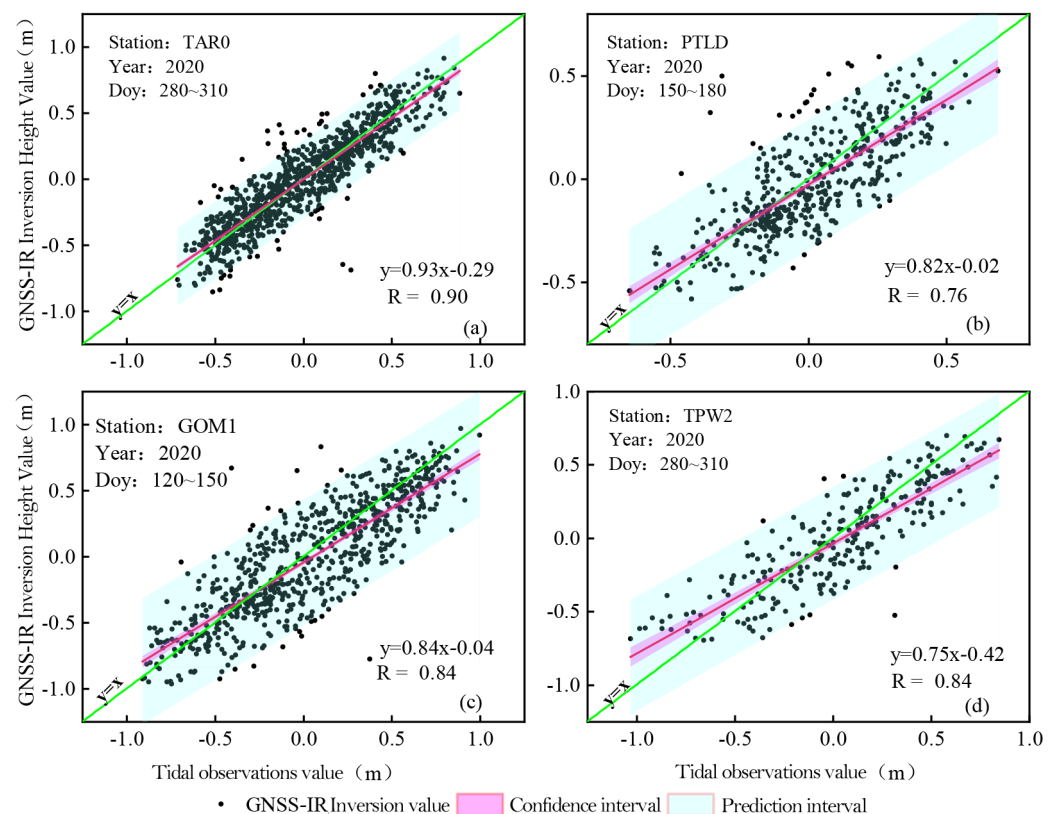
Figure 7. Pearson correlation coefficient between the inverted height sequence after correction using the ionospheric stratified elevation angle correction model and the observed tidal sequence value: (**a**) Image of the correlation coefficient for TAR0; (**b**) Image of the correlation coefficient for PTLD; (**c**) Image of the correlation coefficient for GOM1; (**d**) Image of the correlation coefficient for TPW2.

A comparative study of sea surface height measurements that have not been corrected by ionospheric refraction and that have been corrected by the ISEACM method is conducted. Figure 7 shows the comparison of height inversion results with tide values before and after

the new ISEACM method of correction for the four stations for one month, while Table 2 lists detailed RMSE and PCC comparisons before and after the model modification for the four stations.

Table 2. Root mean square error and Pearson correlation coefficient before and after the correction of ionospheric stratified elevation angle correction model.

Station	RMSE before Correction (m)	PCC before Correction	RMSE after Correction (m)	PCC after Correction
TAR0	0.1752	0.88	0.1493	0.90
PTLD	0.2041	0.72	0.1732	0.76
GOM1	0.2654	0.82	0.2480	0.84
TPW2	0.2616	0.81	0.2178	0.83

From the observations in Figure 8 and Table 2, it is evident that the number of height sequences derived from GNSS-IR sea surface height inversion without the ISEACM correction is fewer compared to those corrected for ionospheric refraction. Furthermore, the height inversion values corrected for ionospheric refraction align more closely with tidal observations, exhibiting significantly better correlation. By comparing the root mean square error and correlation coefficient before and after ISEACM correction of the four stations in Table 2, it is found that the RMSE of the ISEACM model is up to 20% compared with the traditional GNSS-IR sea surface altimetry, and the Pearson correlation coefficient is 4% higher than the traditional GNSS-IR sea surface altimetry.
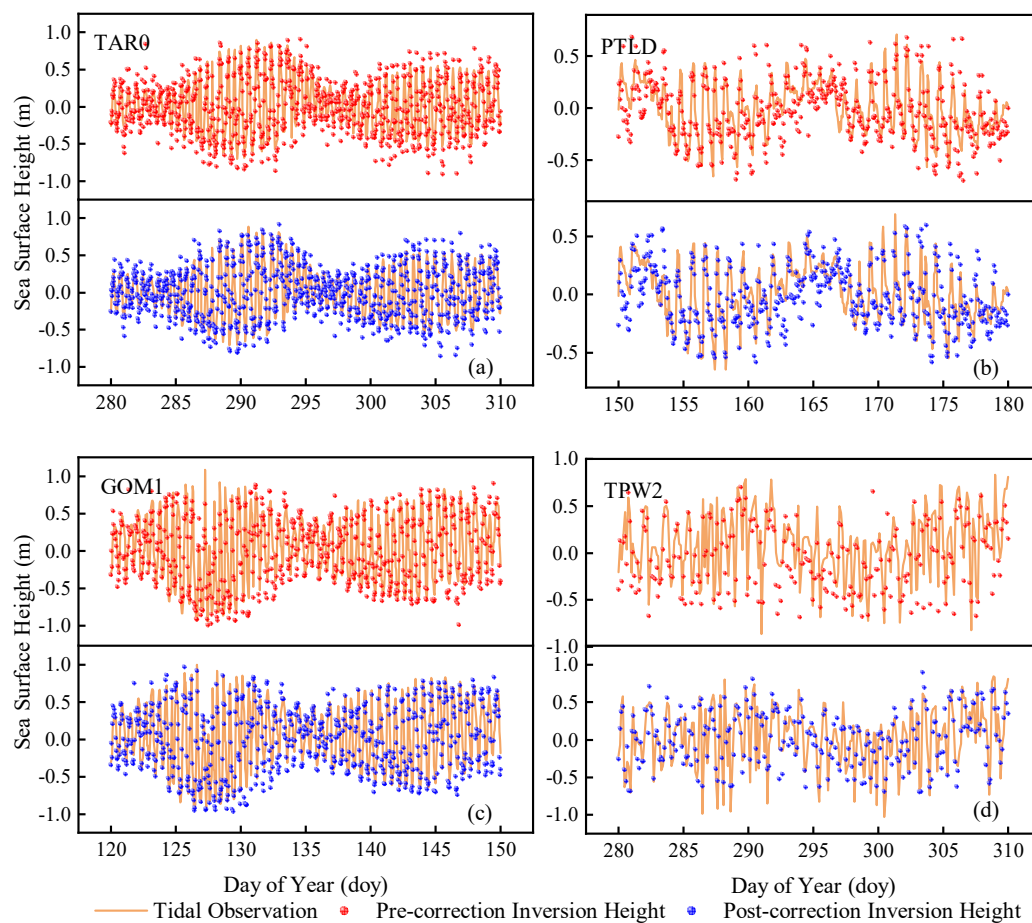
Figure 8. Comparison of height inversion sequences and tidal observation sequences before and after correction by the ionospheric stratified elevation angle correction model for four stations: (**a**) TAR0 station; (**b**) PTLD station; (**c**) GOM1 station; (**d**) TPW2 station.

Based on the residual plots before and after the correction of ionospheric refraction angles in Figure 9, it is evident that the precision of GNSS-IR sea surface height estimation significantly improves after applying ISEACM correction across the four stations. This validates the impact of ionospheric refraction on elevation angles, ultimately leading to accuracy degradation in GNSS-IR sea surface height inversion. Therefore, utilizing ISEACM to correct satellite elevation angles is both feasible and effective in enhancing the accuracy of final GNSS-IR sea surface height inversion.
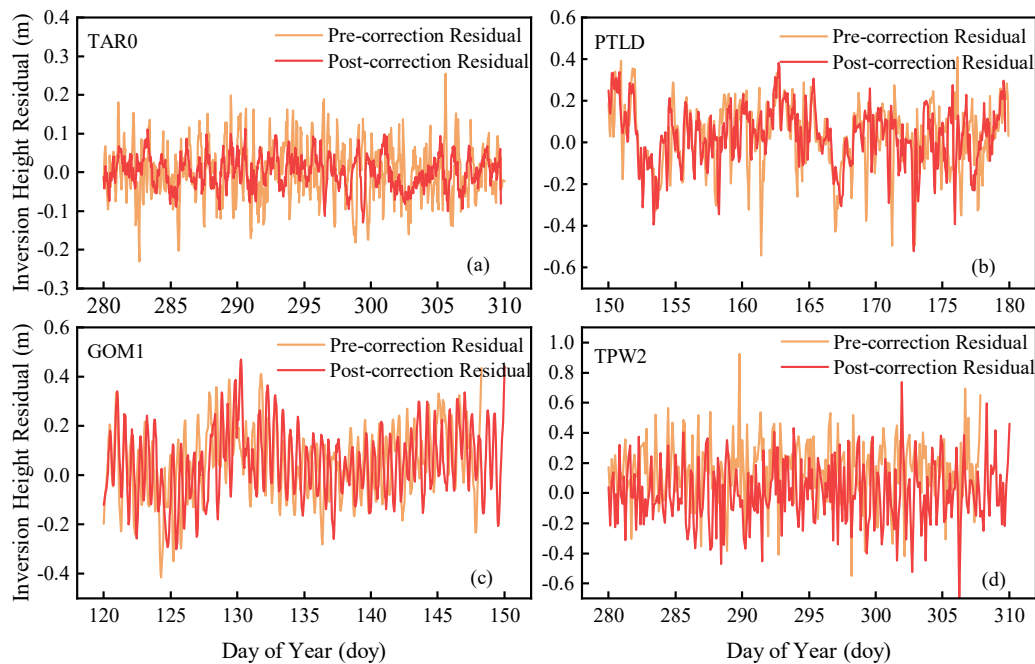
Figure 9. Comparison of residual plots between height inversion sequences and tidal observation sequences before and after correction by the ionospheric stratified elevation angle correction model for four stations: (**a**) Residual image of TAR0; (**b**) Residual image of PTLD; (**c**) Residual image of GOM1; (**d**) Residual image of TPW2.

4. Conclusions

Current research in GNSS-IR sea surface height measurement faces a significant challenge: when GNSS signals pass through the ionosphere, they are affected by the ionospheric electron content density, which causes the satellite signals to refract, thus affecting the calculation results of the satellite elevation angle measured by the measuring station, reducing the accuracy of the altitude angle measurement, and finally affecting the accuracy of the GNSS-IR sea surface altimetry results. In order to solve this problem, a new ionospheric stratified elevation angle correction model is proposed in this study, aiming at the refraction of satellite signals in the ionosphere of GNSS-IR sea surface measurement, which improves the accuracy of GNSS-IR sea surface altitude inversion. The main contributions of this study are as follows:

(1)   A new ionospheric stratification elevation angle correction model has been developed to address the ionospheric refraction issues in current satellite altimetry. In this study, the uneven distribution of ionospheric electron density at different altitudes throughout the entire GNSS-IR sea surface height retrieval process results in varying degrees of elevation angle deviation in satellite signals due to refraction. Therefore, a stratified approach has been introduced to mitigate these effects. The IRI model is used to extract the electron content density at different times, latitudes and longitudes, and ionospheric corresponding layering heights, then the elevation angle correction is calculated by using the ray trace method, and finally, the purpose of improving the accuracy of GNSS-IR sea surface height inversion is achieved.

(2) The feasibility of the proposed ISEACM was validated through comparative analysis with tide gauge station data. Four GNSS satellite stations, TAR0, GOM1, PTLD, and TPW2, were selected to correct the satellite altitude angle by using a new ionospheric stratified elevation angle correction model, and then the GNSS-IR sea surface height measurement results were calculated and compared with the tide gauge data. The results indicate a strong correlation exceeding 0.75 between GNSS-IR sea surface height measurements corrected using ISEACM and tide gauge station data. The root mean square error was maintained within 0.30 m. These results show that the proposed ISEACM has good accuracy and reliability in the estimation of sea surface height.

(3) A comparative study was conducted between conventional GNSS-IR sea surface height measurements and those corrected using the ISEACM model, aiming to analyze the superiority of the ISEACM model. The comparative analysis reveals that the ISEACM model enhances the accuracy of GNSS-IR sea surface height retrieval by up to 20% at its peak and 7% at its minimum compared to traditional methods. On average, the ISEACM model achieves a Pearson correlation coefficient of 0.84, representing a 4% increase over traditional GNSS-IR sea surface height retrieval methods. Therefore, the ISEACM model has optimized, to some extent, the satellite elevation angle errors induced by ionospheric refraction, thereby enhancing the accuracy of sea surface height measurements.

While ISEACM has achieved promising results in ionospheric refraction correction, the method still exhibits certain limitations. It involves intricate calculus operations, offering high precision but demanding extensive computational resources due to its multiple iterations and computational overhead. Currently, its application is predominantly in post-processing experimental scenarios. Future advancements could explore faster correction methods to enhance real-time capabilities for GNSS-IR sea surface height experiments. Additionally, since GNSS-IR shore-based stations are stationary, they are susceptible to environmental factors such as marine vessels, wind speeds, and nearby structures, which can introduce errors. Future efforts could focus on identifying and filtering out these sources of error to improve the accuracy of sea surface height retrieval. Furthermore, ongoing research is exploring airborne and shipborne GNSS-IR systems, which could mitigate environmental impacts around fixed stations.

Author Contributions: Conceptualization, J.Z.; methodology, J.Z. and Y.S.; software, J.Z.; validation, J.Z.; formal analysis, J.Z. and Y.S.; investigation, J.Z.; resources, J.Z. and Y.S.; data curation, J.Z. and Y.S.; writing—original draft, J.Z.; writing—review and editing, W.Z., Y.S., K.X. and H.Z.; supervision, W.Z., Y.S., K.X. and H.Z.; project administration, W.Z.; funding acquisition, W.Z. All authors have read and agreed to the published version of the manuscript.

Data Availability Statement: The GNSS observation data are from SONEL: https://www.sonel.org (accessed on 28 May 2024); the tide gauge dataset can be obtained from UNESCO: http://www.ioc-sealevelmonitoring.org/map.php (accessed on 28 May 2024); and the electron content density data used in this study came from the IRI: https://ccmc.gsfc.nasa.gov/models/IRI~2016 (accessed on 28 May 2024).

References

1. Sun, M.; Feng, W.; Yu, D.; Chen, X.; Liang, W.; Zhong, M. Analysing the impact of SWOT observation errors on marine gravity recovery. *Geophys. J. Int.* **2024**, *237*, 862–871. [CrossRef]

2. Sandwell, D.T.; Smith, W.H.F.; Gille, S.; Kappel, E.; Jayne, S.; Soofi, K.; Coakley, B.; Geli, L.; Cazenave, A.; Boucher, C. Bathymetry from space; rationale and requirements for a new, high-resolution altimetric mission. *Comptes Rendus. Geosci.* **2006**, *338*, 1049–1062. [CrossRef]

3. Li, Z.; Guo, J.; Ji, B.; Wan, X.; Zhang, S. A Review of Marine Gravity Field Recovery from Satellite Altimetry. *Remote Sens.* **2022**, *14*, 4790. [CrossRef]

4. Hu, Y.; Yuan, X.; Liu, W.; Wickert, J.; Jiang, Z.; Haas, R. GNSS-IR Model of Sea Level Height Estimation Combining Variational Mode Decomposition. *IEEE J. Sel. Top. Appl. Earth Observ. Remote Sens.* **2021**, *14*, 10405–10414. [CrossRef]

5. AGU. Launching of United States Vanguard satellite. *J. Geophys. Res.* **1958**, *63*, 423.

6. Hofmann-Wellenhof, B.; Lichtenegger, H.; Wasle, E. *GNSS—Global Navigation Satellite Systems: GPS, GLONASS, Galileo, and More*; Springer: New York, NY, USA; Wien, Austria, 2008.

7. Martin-Neira, M. A passive reflectometry and interferometry system (PARIS):application to ocean altimetry. *ESA J.* **1993**, *17*, 331–355.

8. Auber, J.C.; Bilbaut, A.; Rigal, J.M. Characterization of Multipath on Land and Sea at GPS Frequencies. In Proceedings of the 7th International Technical Meeting of the Satellite Division of the Institute of Navigation (Ion Gps 1994), Alexandria, VA, USA, 20–23 September 1994; pp. 1155–1171.

9. Lowe, S.T.; LaBrecque, J.L.; Zuffada, C.; Romans, L.J.; Young, L.E.; Hajj, G.A. First spaceborne observation of an Earth-reflected GPS signal: First spaceborne observations of an earth-reflected GPS signal. *Radio Sci.* **2002**, *37*, 7. [CrossRef]

10. Hajj, G.A.; Zuffada, C. Theoretical description of a bistatic system for ocean altimetry using the GPS signal. *Radio Sci.* **2003**, *38*, 1089. [CrossRef]

11. Martin-Neira, M.; Caparrini, M.; Font-Rossello, J.; Lannelongue, S.; Vallmitjana, C.S. The PARIS concept: An experimental demonstration of sea surface altimetry using GPS reflected signals. *IEEE Trans. Geosci. Remote Sens.* **2001**, *39*, 142–150. [CrossRef]

12. Caparrini, M.; Ruffini, L.; Ruffini, G. PARFAIT: GNSS-R coastal altimetry. *arXiv* **2003**, arXiv:physics/0311052.

13. Rivas, M.B.; Martin-Neira, M. Coherent GPS reflections from the sea surface. *IEEE Geosci. Remote Sens. Lett.* **2006**, *3*, 28–31.

14. Yan, Z.; Zheng, W.; Wu, F.; Wang, C.; Zhu, H.; Xu, A. Correction of Atmospheric Delay Error of Airborne and Spaceborne GNSS-R Sea Surface Altimetry. *Front. Earth Sci.* **2022**, *10*, 730551. [CrossRef]

15. Gleason, S.; Hodgart, S.; Sun, Y.; Gommenginger, C.; Mackin, S.; Adjrad, M.; Unwin, M. Detection and Processing of bistatically reflected GPS signals from low Earth orbit for the purpose of ocean remote sensing. *IEEE Trans. Geosci. Remote Sens.* **2005**, *43*, 1229–1241. [CrossRef]

16. Clifford, S.F.; Tatarskii, V.I.; Voronovich, A.G.; Zavorotny, V.U. GPS sounding of ocean surface waves: Theoretical assessment. In Proceedings of the IGARSS'98. Sensing and Managing the Environment, 1998 IEEE International Geoscience and Remote Sensing. Symposium Proceedings, Seattle, WA, USA, 6–10 July 1998; Volume 4.

17. Zavorotny, V.U.; Voronovich, A.G. Scattering of GPS signals from the ocean with wind remote sensing application. *IEEE Trans. Geosci. Remote Sens.* **2000**, *38*, 951–964. [CrossRef]

18. Foti, G.; Gommenginger, C.; Jales, P.; Unwin, M.; Shaw, A.; Robertson, C.; Roselló, J. Spaceborne GNSS reflectometry for ocean winds: First results from the UK TechDemoSat-1 mission. *Geophys. Res. Lett.* **2015**, *42*, 5435–5441. [CrossRef]

19. Clarizia, M.P.; Ruf, C.; Cipollini, P.; Zuffada, C. First spaceborne observation of sea surface height using GPS-Reflectometry. *Geophys. Res. Lett.* **2016**, *43*, 767–774. [CrossRef]

20. Li, W.; Cardellach, E.; Fabra, F.; Rius, A.; Ribó, S.; Martín Neira, M. First spaceborne phase altimetry over sea ice using TechDemoSat-1 GNSS-R signals. *Geophys. Res. Lett.* **2017**, *44*, 8369–8376. [CrossRef]

21. Jin, S.; Najibi, N. Sensing snow height and surface temperature variations in Greenland from GPS reflected signals. *Adv. Space Res.* **2014**, *53*, 1623–1633. [CrossRef]

22. McCreight, J.L.; Small, E.E.; Larson, K.M. Snow depth, density, and SWE estimates derived from GPS reflection data; validation in the Western U.S. *Water Resour. Res.* **2014**, *50*, 6892–6909. [CrossRef]

23. Hu, Y.; Qu, W.; Liu, W.; Yuan, X. GNSS-R snow depth retrieval algorithm based on PSO-LSTM. *Meas. Sci. Technol.* **2024**, *35*, 65801. [CrossRef]

24. Gleason, S. *Remote Sensing of Ocean, Ice and Land Surfaces Using Bistatically Scanner GNSS Signals from Low Earth Orbit*; ProQuest Dissertations Publishing: Ann Arbor, MI, USA, 2006.

25. Xie, Y.; Yan, Q. Stand-Alone Retrieval of Sea Ice Thickness From FY-3E GNOS-R Data. *IEEE Geosci. Remote Sens. Lett.* **2024**, *21*, 1–5. [CrossRef]

26. Rodriguez-Alvarez, N.; Francesc Munoz-Martin, J.; Bosch-Lluis, X.; Oudrhiri, K. Full Polarimetric GNSS-R Assessment of the Freeze and Thaw States of the Terrestrial Cryosphere. *IEEE Trans. Geosci. Remote Sens.* **2024**, *62*, 1–11. [CrossRef]

27. Li, C.; Huang, W. Sea surface oil slick detection from GNSS-R Delay-Doppler Maps using the spatial integration approach. In Proceedings of the 2013 IEEE Radar Conference, Ottawa, ON, Canada, 29 April–3 May 2013; pp. 1–6.

28. Chen, Y.; Yan, S.; Gong, J. Phase Error Analysis and Compensation of GEO-Satellite-Based GNSS-R Deformation Retrieval. *IEEE Geosci. Remote Sens. Lett.* **2022**, *19*, 1–5. [CrossRef]

29. Zhang, Y.; Chen, S.; Hong, Z.; Han, Y.; Li, B.; Yang, S.; Wang, J.; Seya, H. Feasibility of Oil Slick Detection Using BeiDou-R Coastal Simulation. *Math. Probl. Eng.* **2017**, *2017*, 8098029. [CrossRef]

30. Yan, Q.; Liu, S.; Chen, T.; Jin, S.; Xie, T.; Huang, W. Mapping Surface Water Fraction Over the Pan-Tropical Region Using CYGNSS Data. *IEEE Trans. Geosci. Remote Sens.* **2024**, *62*, 1–14. [CrossRef]

31. Yanez, C.; Li, W.; Cardellach, E.; Raynal, M.; Picot, N.; Martin-Neira, M.; Borde, F. Lake Water Level Estimation From Grazing GNSS-Reflectometry and Satellite Radar Altimetry Over the Great Lakes. *IEEE Geosci. Remote Sens. Lett.* **2024**, *21*, 1–5. [CrossRef]

32. Chew, C.; Shah, R.; Zuffada, C.; Hajj, G.; Masters, D.; Mannucci, A.J. Demonstrating soil moisture remote sensing with observations from the UK TechDemoSat-1 satellite mission. *Geophys. Res. Lett.* **2016**, *43*, 3317–3324. [CrossRef]

33. Perez-Portero, A.; Rodriguez-Alvarez, N.; Munoz-Martin, J.F.; Bosch-Lluis, X.; Oudrhiri, K. Estimating Backward Scattering Using GNSS-Reflectometry Measurements for Soil Moisture Retrieval. *IEEE Access.* **2024**, *12*, 73608–73619. [CrossRef]

34. Edokossi, K.; Calabia, A.; Jin, S.; Molina, I. GNSS-Reflectometry and Remote Sensing of Soil Moisture: A Review of Measurement Techniques, Methods, and Applications. *Remote Sens.* **2020**, *12*, 614. [CrossRef]

35. Fabra, F.; Cardellach, E.; Rius, A.; Ribo, S.; Oliveras, S.; Nogues-Correig, O.; Rivas, M.B.; Semmling, M.; D'Addio, S. Phase Altimetry with Dual Polarization GNSS-R Over Sea Ice. *IEEE Trans. Geosci. Remote Sens.* **2012**, *50*, 2112–2121. [CrossRef]

36. Li, Y.; Yu, K.; Jin, T.; Chang, X.; Wang, Q.; Li, J. Development of a GNSS-IR instrument based on low-cost positioning chips and its performance evaluation for estimating the reflector height. *Gps Solut.* **2021**, *25*, 127. [CrossRef]

37. Wang, X.; Zhang, Q.; Zhang, S. Water levels measured with SNR using wavelet decomposition and Lomb–Scargle periodogram. *Gps Solut.* **2018**, *22*, 2. [CrossRef]

38. Larson, K.M.; Löfgren, J.S.; Haas, R. Coastal sea level measurements using a single geodetic GPS receiver. *Adv. Space Res.* **2013**, *51*, 1301–1310. [CrossRef]

39. Loefgren, J.S.; Haas, R.; Scherneck, H.; International, A.O.G.I.; Pagiatakis, S.; Bogusz, J. Sea-level time series and ocean-tide analysis from multipath signals at five GPS sites in different parts of the world. *J. Geodyn.* **2014**, *80*, 66–80. [CrossRef]

40. Santamaría-Gómez, A.; Watson, C. Remote leveling of tide gauges using GNSS reflectometry: Case study at Spring Bay, Australia. *Gps Solut.* **2017**, *21*, 451–459. [CrossRef]

41. Larson, K.M.; Ray, R.D.; Williams, S.D.P. A 10-Year Comparison of Water Levels Measured with a Geodetic GPS Receiver Versus a Conventional Tide Gauge. *J. Atmos. Ocean. Technol.* **2017**, *34*, 295–307. [CrossRef]

42. Williams, S.D.P.; Nievinski, F.G. Tropospheric delays in ground-based GNSS multipath reflectometry; experimental evidence from coastal sites. *J. Geophys. Research. Solid Earth* **2017**, *122*, 2310–2327. [CrossRef]

43. Hoque, M.M.; Jakowski, N. Ionospheric propagation effects on GNSS signals and new correction approaches. *Glob. Navig. Satell. Syst. Signal Theory Appl.* **2012**, *10*, 30090.

44. Hernández-Pajares, M.; Roma-Dollase, D.; Garcia-Fernàndez, M.; Orus-Perez, R.; García-Rigo, A. Precise ionospheric electron content monitoring from single-frequency GPS receivers. *Gps Solut.* **2018**, *22*, 102. [CrossRef]

45. Hoque, M.M.; Jakowski, N. An alternative ionospheric correction model for global navigation satellite systems. *J. Geodesy.* **2015**, *89*, 391–406. [CrossRef]

46. Richards, P.G. Seasonal and solar cycle variations of the ionospheric peak electron density: Comparison of measurement and models. *J. Geophys. Res.* **2001**, *106*, 12803–12819. [CrossRef]

47. Petrie, E.J.; Hernández-Pajares, M.; Spalla, P.; Moore, P.; King, M.A. A Review of Higher Order Ionospheric Refraction Effects on Dual Frequency GPS. *Surv. Geophys.* **2011**, *32*, 197–253. [CrossRef]

48. Jiang, C.; Wang, B. Atmospheric refraction corrections of radiowave propagation for airborne and satellite-borne radars. *Sci. China. Technol. Sci.* **2001**, *44*, 280–290. [CrossRef]

49. Lv, J.; Zhang, R.; Tu, J.; Liao, M.; Pang, J.; Yu, B.; Li, K.; Xiang, W.; Fu, Y.; Liu, G. A GNSS-IR Method for Retrieving Soil Moisture Content from Integrated Multi-Satellite Data That Accounts for the Impact of Vegetation Moisture Content. *Remote Sens.* **2021**, *13*, 2442. [CrossRef]

50. Bilich, A.; Larson, K.M.; Axelrad, P. Observations of Signal-to-Noise Ratios (SNR) at Geodetic GPS Site CASA: Implications for Phase Multipath. *Cent. Eur. Geodyn. Seismol.* **2004**, *23*, 77–83.

51. Carolyn, R.; Kristine, M.L. Software tools for GNSS interferometric reflectometry (GNSS-IR). *Gps Solut.* **2018**, *22*, 80.

52. Wei, Z.; Ren, C.; Liang, X.; Liang, Y.; Yin, A.; Liang, J.; Yue, W. Sea-Level Estimation from GNSS-IR under Loose Constraints Based on Local Mean Decomposition. *Sensors* **2023**, *23*, 6540. [CrossRef] [PubMed]

53. Guojun, H.; Li, Z.; Gang, L. Research on error analysis and correction technique of atmospheric refraction for InSAR measurement with distributed satellites. *J. Comput. Commun.* **2016**, *4*, 142–150.

54. Chai, T.; Draxler, R.R. Root mean square error (RMSE) or mean absolute error (MAE)?—Arguments against avoiding RMSE in the literature. *Geosci. Model Dev.* **2014**, *7*, 1247–1250. [CrossRef]
55. Shen, Y.; Zheng, W.; Yin, W.; Xu, A.; Zhu, H.; Wang, Q.; Chen, Z. Improving the inversion accuracy of terrestrial water storage anomaly by combining GNSS and LSTM algorithm and its application in mainland China. *Remote Sens.* **2022**, *14*, 535. [CrossRef]